Received 26 January 2015; revised 30 March 2015; accepted 10 April 2015. Date of publication 15 April 2015; date of current version 19 June 2015.
The review of this paper was arranged by Editor A. G. U. Perera.

Digital Object Identifier 10.1109/JEDS.2015.2423233

An Improved Model for the Full Well Capacity in Pinned Photodiode CMOS Image Sensors

CHEN CAO[1], BENLAN SHEN[2], BING ZHANG[1], LONGSHENG WU[1], AND JUNFENG WANG[1]

1 Department of Integrated Circuit Design, Institute of Microelectronics Technology, Xi'an 710071, China
2 Department of Visual Device, LUSTER Light Tech. Corporation, Beijing 100195, China

CORRESPONDING AUTHOR: C. CAO (e-mail: intercaochen@163.com)

ABSTRACT An improved analytical model for quantifying the full well capacity in pinned photodiode (PPD) CMOS image sensors is proposed. The model captures the characteristics of the realistic technology-induced vertical doping nonuniformity in photon sensing N-type area of the PPD structure and the voltage dependency of the PPD capacitance, respectively, both of which were neglected in the existing works. Excellent agreement between measured and predicted data shows that the proposed model fits a wider range of technology conditions for a wider spectra responding compared to the up-to-date reported model.

INDEX TERMS CMOS image sensors, full well capacity (FWC), pinned photodiode (PPD), analytical model.

I. INTRODUCTION

The Pinned photodiode (PPD) has been widely employed by the state-of-the-art CMOS image sensor (CIS) based on its strong superiority of the dark noise reduction [1]. The full well capacity (FWC) represents the maximum amount of charge that can be accumulated on the PPD capacitance C_{PPD}. It is thus of great importance to determine the pixel output voltage swing and even the overall sensor performance [2]. Analytical predictions of the FWC are tremendously demanded to provide optimization design guides to meet the development of the PPD-CIS. Recently, an outstanding FWC model [2] was developed based on a series of former works [3]–[5] by capturing the characteristic of the FWC dependence on the photon flux under both states of the transfer gate transistor (TG) depleted and accumulated. However, the above work has a limitation on physical description of the PPD capacitance (which fundamentally determines the FWC) by regarding C_{PPD} as a constant. But actually on the one hand, the technology-induced vertical doping non-uniformity in the photon sensing N-type area of a PPD can influence C_{PPD} spatially for one-dimension. On the other hand, the voltage dependency of C_{PPD}, which has been demonstrated in [6], can also influence C_{PPD} during integration time. In order to feature the important characteristics described above, the needs of the improved modeling works are getting increased.

In this work, a novel analytical model for predicting the PPD FWC is developed by considering the influences of the doping-dependent and voltage-dependent C_{PPD} on the estimation of the FWC in detail. The model is experimentally verified to be valid and universal under a wider range of N-type doping conditions compared to the up-to-date reported model.

II. MODEL DEVELOPMENT

The PPD-CIS based pixel (normally called 4T-pixel) presented in Fig. 1 consists of a PPD with a stack of P^+/N/P-epi structure and four functional transistors. The operation principle of the 4T-pixel was detailed in [7]. The PPD which connected to a floating diffusion (FD) node by the TG is modeled by using Sentaurus TCAD Process tools based on the deep sub-micrometer (DSM) CIS technology. It is observed that, owing to the fact the impurity compensation between donors and acceptors can occur smoothly during the processes of ion implantations and subsequent thermal anneals, the doping distribution in the photon sensing N-type area of the PPD presents non-uniformity and vertical attenuation. According to the highly wavelength dependency of

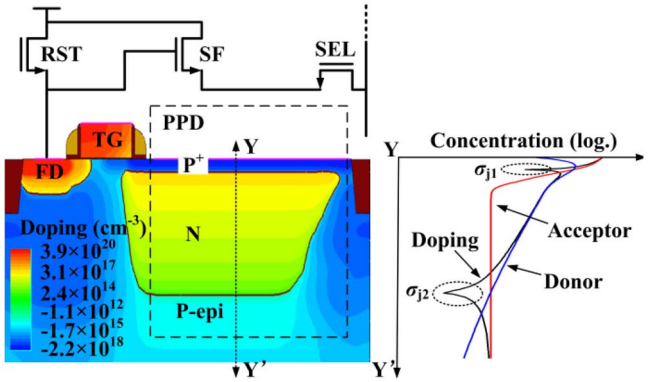

FIGURE 1. 4T-pixel with process-modeled doping distributions of the PPD and TG. The doping profile along Y-Y' is shown as well, in which the σ_{j1} and the σ_{j2} are the deceasing gradients (calculated from slopes) of the doping levels at the metallurgical junctions of P^+/N and N/P-epi, respectively.

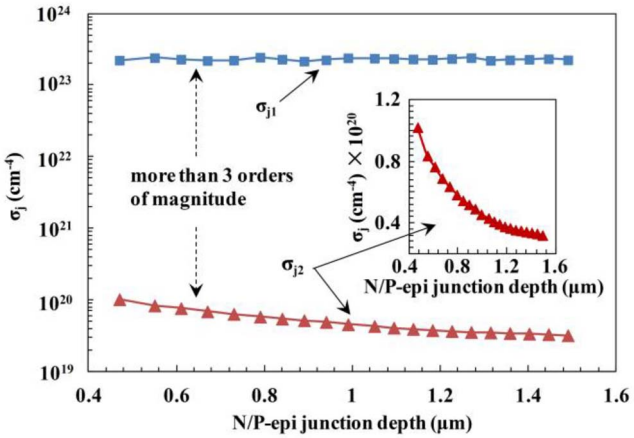

FIGURE 2. Simulated σ_{j1} and σ_{j2} (both defined in Fig. 1) versus N/P-epi junction depth based on the Fig. 1's PPD model. The inset shows a clear σ_{j2} behavior in linear expression.

photon absorption depth $d_{PH}(\lambda)$ in silicon material, which is described empirically as [8]

$$d_{PH}(\lambda) = \alpha^{-1} = \left(\frac{84.732}{\lambda} - 76.417\right)^{-2} \tag{1}$$

where α is the photon absorption coefficient with units of cm^{-1}, we can easily deduce that the visible light at the wavelength generally between 300nm and 700nm could be absorbed effectively at the depth between 0.24μm and 5μm. That means the N/P-epi junction particular for the longer wavelength responding in a PPD should be deepened properly for a wider spectra responding, thus manifesting the N-type doping non-uniformity because a more thorough donor-acceptor compensation would occur close to the N/P-epi junction.

It is difficult to analytically estimate the N-type doping non-uniformity straightforwardly due to the complicated doping profile created by the local donor-acceptor compensation, as shown in Fig. 1. In our FWC modeling work, we focus on pursuing a simple yet alternative method to capture the effect of the N-type doping behavior on C_{PPD}. As shown in Fig. 2, the difference between the σ_{j1} and the σ_{j2} resulted from the non-uniformity of N-type doping is generally more than 3 orders of magnitude and even larger as the N/P-epi junction deepens, resulting in different doping properties between the P^+/N and the N/P-epi junctions, which can be distinguished as abrupt and linear graded, respectively. Therefore, we actually use an equivalent method by accurately modeling the doping properties of the P^+/N and N/P-epi junctions caused by the phenomenon of the N-type doping non-uniformity to perform the modeling of the non-uniform doping profile along the vertical direction. Then, the vertical widths of the two depletion regions formed on both junctions can be expressed as [9]

$$W_{P^+/N}(V) = \left[\frac{2\varepsilon_r\varepsilon_0(\phi_{bi1} + V)}{qN_{N-MAX}}\right]^{\frac{1}{2}} \tag{2}$$

$$W_{N/P-epi}(V) = \left[\frac{12\varepsilon_r\varepsilon_0(\phi_{bi2} + V)}{q\sigma_{j2}}\right]^{\frac{1}{3}} \tag{3}$$

where $\varepsilon_r\varepsilon_0$ is the dielectric constant of silicon, N_{N-MAX} is the peak N-type doping level, q is the charge element. The σ_{j2} here is the item which can reflect indeed the N-type doping non-uniformity. ϕ_{bi1} and ϕ_{bi2} are the equilibrium built-in potentials across both junctions, respectively, their values are highly doping profile dependencies, which can be expressed as

$$\phi_{bi1} = \frac{k_0T}{q} \cdot \ln\frac{N_{N-MAX}N_{P^+}}{n_i^2} \tag{4}$$

$$\phi_{bi2} = \frac{k_0T}{q} \cdot \ln\frac{N_{N-MIN}N_{P-epi}}{n_i^2} \tag{5}$$

where N_{N-MIN} is the donor concentration of the infinite small N-type region close to the position of the N/P-epi metallurgical junction, and can be approximately equal to N_{P-epi} (referred to the concentration of the epitaxial layer) in terms of the behavior of the linear graded junction. To keep our model as simple as possible, the lateral depletion of the N-type has been neglected, hence C_{PPD} consists of two plate-like junction capacitors established by the vertical depletion regions, and can be expressed as

$$C_{PPD}(V) = A_{PPD}\varepsilon_r\varepsilon_0 \cdot \left(\frac{1}{W_{P^+/N}(V)} + \frac{1}{W_{N/P-epi}(V)}\right) \tag{6}$$

where A_{PPD} is the photon sensing area of the PPD. It is indicated that, the biasing dependencies of both the depletion widths result in the highly voltage dependency of C_{PPD} during integration time, causing C_{PPD} variable under illumination. Ultimately, the FWC N_{FW} can be estimated as the product of C_{PPD} and the maximum voltage swing across the PPD, which should depend on the integral of the voltage

from the doping dependent pinch-off level V_{pin} [10] to the saturation level V_{FW}

$$N_{\mathrm{FW}} = -\frac{1}{q}\int_{V_{\mathrm{pin}}}^{V_{\mathrm{FW}}} C_{\mathrm{PPD}}(V)\,dV = A_{\mathrm{PPD}}\left\{\left(\frac{2\varepsilon_{\mathrm{r}}\varepsilon_0 N_{\mathrm{N-MAX}}}{q}\right)^{\frac{1}{2}}\left[\left(V_{\mathrm{pin}}+\phi_{\mathrm{bi1}}\right)^{\frac{1}{2}} - \left(V_{\mathrm{FW}}+\phi_{\mathrm{bi1}}\right)^{\frac{1}{2}}\right] + \left(\frac{9\varepsilon_{\mathrm{r}}^2\varepsilon_0^2\sigma_{\mathrm{j2}}}{32q^2}\right)^{\frac{1}{3}}\left[\left(V_{\mathrm{pin}}+\phi_{\mathrm{bi2}}\right)^{\frac{2}{3}} - \left(V_{\mathrm{FW}}+\phi_{\mathrm{bi2}}\right)^{\frac{2}{3}}\right]\right\}. \tag{7}$$

Notice that equation (7) consists of two sub-expressions, which refer to the charge capacities of the P^+/N junction capacitor and the N/P-epi junction capacitor, respectively. The dependences of each charge capacity on both the N-type doping property and the PPD voltage are clarified within each sub-expression. The V_{FW} can be calculated as a function of photon flux Φ_{PH} thanks to the Pelamatti's theoretical work [2] as following

$$V_{\mathrm{FW}}(\Phi_{\mathrm{PH}}) = -v_{\mathrm{th}}\ln\left(\frac{\eta\Phi_{\mathrm{PH}}+I_{\mathrm{sat}}}{I_{\mathrm{sat}}}\right) \tag{8}$$

where v_{th} is the thermal voltage, $\eta\Phi_{\mathrm{PH}}$ is the photocurrent with η being an efficiency factor<1, I_{sat} is the photodiode reverse current. The sub-threshold current of the TG has been neglected in equation (8) by biasing the TG off-voltage to -0.5V in this work, such that the TG channel would keep accumulated during integration time. It is expected that the proposed model would follow the characteristic of photon flux dependency well by holding the estimation mechanism of V_{FW} reported in [2].

III. EXPERIMENTAL DETAILS

For the model verification, a well-designed test chip constituted of multiple 10×10 6μm-pitch 4T-pixel sub-arrays with various PPD-N-type implant conditions (different pairs of dose and energy levels) was fabricated using a DSM 1P4M CIS dedicated technology. The epitaxial layer with a concentration of $10^{15}\mathrm{cm}^{-3}$ was grown on the P-type conductive substrate. The micrograph of the chip is shown in Fig. 3(a). The details of the manufactured pixels with variable N-type processes are presented in Table 1. The related parameters $N_{\mathrm{N-MAX}}$ and σ_{j2}, extracted out by C-V methods [9], have been listed as well for the model calculation. Each pixel element of one sub-array can be accessed by performing the classical 4T-pixel control timing scheme [11] with correlated double sampling. The chip output is the digital signal (DN) that converted by a 14-bit analog to digital convertor. Then, the amount of photo-charge accumulated in the accessed PPD can be easily obtained by dividing the conversion gain,

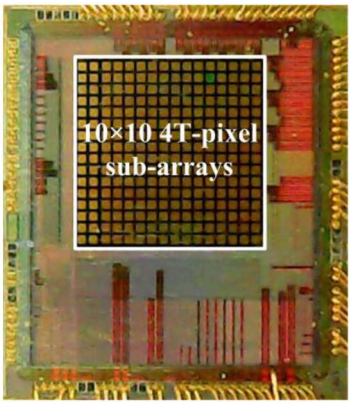

(a)

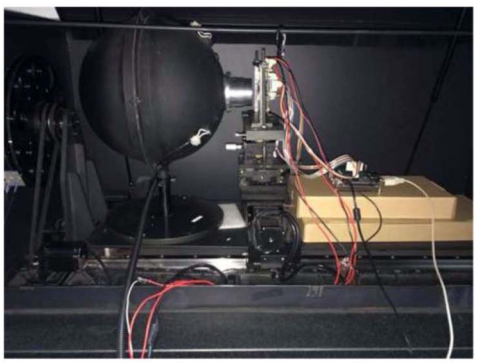

(b)

FIGURE 3. **(a) Test chip micrograph. (b) Photoelectric experimental environment.**

TABLE 1. **Summary of variable N-type implant conditions and extracted values of model parameters.**

Dose (cm^{-2}) ×10^{12}	Energy (keV)	$N_{\mathrm{N-MAX}}$ (cm^{-3}) ×10^{17}	σ_{j2} (cm^{-4}) ×10^{19}
2.0		0.47	5.96
3.0		0.78	5.93
4.0		1.18	5.88
5.0		1.63	5.83
6.0	100	2.09	5.77
7.0		2.57	5.73
8.0		3.06	5.68
9.0		3.54	5.61
10.0		4.02	5.56
	70	1.37	7.65
	80	1.45	6.90
	90	1.55	6.37
	100	1.63	5.83
5.0	110	1.78	5.46
	120	1.66	5.19
	130	1.61	4.92
	140	1.52	4.55
	150	1.44	4.31

which owns a unit of LSB/e^-, from the output DN value. 100 frames were acquired for each sub-array to achieve an accurate signal value. The steady-state monochromatic illumination with an adjustable photon flux was generated by an integrating sphere. The measurement was performed at LUSTER Light Tech. Corporation in Beijing, at room

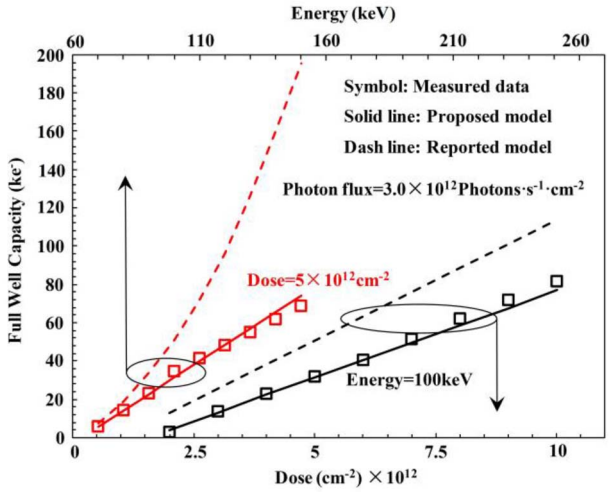

FIGURE 4. **Comparisons of measured data between the proposed and the reported models under two groups of N-type implant conditions. One for doses varying from 2 × 10^{12} to 1 × 10^{13} cm^{-2} with energy of 100 keV, the other for energies varying from 70 to 150 keV with dose of 5 × 10^{12} cm^{-2}. The photon flux has been set to a constant level of 3.0 × 10^{12} Photons · s^{-1} · cm^{-2} with chosen integration times for approaching PPD saturation.**

temperature (≈ 25 °C). The corresponding photograph of the experimental environment is presented in Fig. 3(b).

IV. RESULTS AND DISCUSSION

In order to emphasize more intuitively the doping process dependency of the FWC in this paper to provide a feasible process guidance, the implant dose and energy levels (each pair of them pointed to a specific group of N_{N-MAX} and σ_{j2} data exhibited in Table 1) of the N-type have been directly chosen as the variables to feature the behaviors of the FWC, as shown in Fig. 4. Apparently, it can be observed that the proposed model describes the measured data much better than the reported model in [2] (termed reported model subsequently) under a wider range of N-type implant conditions. Notice that the linear dependencies of the FWC on both implant dose and energy levels result partially from the doping-dependent characteristic of V_{pin}, according to equation (7). A positive deviation of the reported model from the measured data is observed as implant dose or energy increases. The reason can be interpreted that as a result of the absence of the gradient attenuated N-type doping declared in the reported model, a stronger bias should be supplied to exhaust the whole N-type neutral region with much higher concentration, causing an extra level of $\triangle V_{pin}$ must be added in the reported model compared to the V_{pin} in the proposed model. In this case, an increment of the FWC is introduced in terms of the following description

$$N_{FW} + \Delta N_{FW} = -\frac{1}{q}\int_{V_{pin}+\Delta V_{pin}}^{V_{FW}} C_{PPD}\,dV. \qquad (9)$$

A potential diagram comparison illustrated in Fig. 5 facilitates the comprehension of the FWC prediction difference

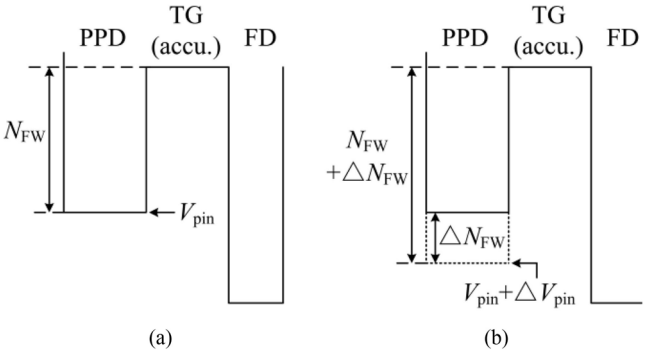

FIGURE 5. **Potential diagram of the PPD, TG, and FD structure within the device during TG accumulated both for (a) proposed model and (b) reported model. The mark "accu." represents accumulated state.**

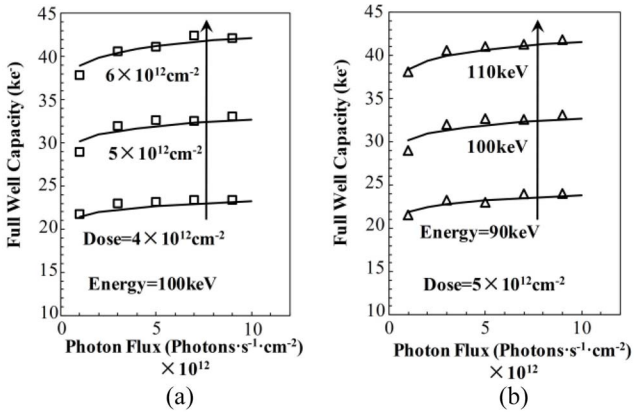

FIGURE 6. **Comparisons of the FWC against incident photon flux of the proposed model with measured data for the N-type implant at (a) doses between 4 × 10^{12} and 6 × 10^{12} cm^{-2} with energy of 100 keV, (b) energies between 90 and 110 keV with dose of 5 × 10^{12} cm^{-2}. Symbols and lines correspond to measured data and the model predictions, respectively.**

between two models. In addition, the reported model rises more rapidly as a quadratic curve with increasing implant energy (caused by the square N-type vertical width dependence of the V_{pin} developed in [12] for uniform N-type doping profile) than with increasing implant dose. This phenomenon explains that the N-type doping non-uniformity can be aggravated by deepening the N/P-epi junction through increasing the N-type implant energy, thus enlarging the prediction difference between two models. Consequently, one primary contribution of the proposed model is to catch accurately the dependency of the FWC on the N-type vertical width, which has not been implemented in former works.

To verify the adaptability of the proposed model to the reported model, the FWC against incident photon flux for a series of different N-type implant dose and energy levels are compared between the measured data and the model predictions in this work [see Fig. 6]. As it can be observed, for each specific implant condition, the predicted curve is well fitted by a logarithmic function as well as what were reported in [2] by means of holding the $V_{FM}(\Phi_{PH})$ item in the proposed model, and shows a good agreement compared to the measurement.

V. CONCLUSION

An improved analytical model of the FWC for the PPD-CIS has been developed. The model precisely captures the vertical non-uniform doping distribution in photon sensing N-type area of a PPD, and the voltage dependency of the PPD capacitance is also included. The validity of the model is demonstrated through the excellent agreement between predicted and measured data for various N-type implant conditions. A wider technology range compatibility of the proposed model is realized compared to the up-to-date reported model, thus can catch the characteristics of the deep junction for a wider spectra responding. The extension of this model to the description of the N-type lateral depletion behavior for a smaller size PPD (such as the one reported in [12]) will be researched in a future work.

ACKNOWLEDGMENT

The authors would like to thank Dr. Y. Zhang and J. L. Liu from LUSTER Light Tech. Corporation and H. Yan from the Institute of Microelectronics Technology, for their supports with the photoelectric experiment operations and fruitful discussion held about pixel-based testing technologies.

REFERENCES

[1] S.-H. Park *et al.*, "Decrease of dark current by reducing transfer transistor induced partition noise with localized channel implantation," *IEEE Electron Device Lett.*, vol. 31, no. 11, pp. 1278–1280, Nov. 2010.

[2] A. Pelamatti, V. Goiffon, M. Estribeau, P. Cervantes, and P. Magnan, "Estimation and modeling of the full well capacity in pinned photodiode CMOS image sensors," *IEEE Electron Device Lett.*, vol. 34, no. 7, pp. 900–902, Jul. 2013.

[3] B. Mheen, Y.-J. Song, and A. Theuwissen, "Negative offset operation of four-transistor CMOS image pixels for increased well capacity and suppressed dark current," *IEEE Electron Device Lett.*, vol. 29, no. 4, pp. 347–349, Apr. 2008.

[4] M. Sarkar, B. Buttgen, and A. Theuwissen, "Feedforward effect in standard CMOS pinned photodiodes," *IEEE Trans. Electron Devices*, vol. 60, no. 3, pp. 1154–1161, Mar. 2013.

[5] J. Bogaerts, G. Meynants, K. Van Wichelen, and E. Gillisjans, "Recent radiation testing on 180 nm and 110 nm CMOS image sensor processes," in *Proc. CNES Workshop Radiat. Effects Optoelectron. Detectors*, Toulouse, France, Nov. 2012.

[6] C. Y. Chao *et al.*, "Extraction and estimation of pinned photodiode capacitance in CMOS image sensors," *IEEE J. Electron Devices Soc.*, vol. 2, no. 4, pp. 59–64, Jul. 2014.

[7] E. R. Fossum and D. B. Hondongwa, "A review of pinned photodiode for CCD and CMOS image sensors," *IEEE J. Electron Devices Soc.*, vol. 2, no. 3, pp. 33–43, May 2014.

[8] G. Adam, "Investigation of 4T CMOS image sensor design and the effects of radiation damage," Ph.D. dissertation, Dept. Phys., Surrey Univ., Guildford, U.K., 2010.

[9] E. Liu, B. Zhu, and J. Luo, *The Physics of Semiconductors*, 7th ed. Beijing, China: Electron. Ind., 2012.

[10] C. Cao, B. Zhang, X. Li, L. Wu, and J. Wang, "Pinch-off voltage modeling for CMOS image pixels with a pinned photodiode structure," *J. Semicond.*, vol. 35, no. 7, Jul. 2014, Art. ID 074012.

[11] V. Goiffon *et al.*, "Pixel level characterization of pinned photodiode and transfer gate physical parameters in CMOS image sensors," *IEEE J. Electron Devices Soc.*, vol. 2, no. 4, pp. 65–76, Jul. 2014.

[12] S. Park and H. Uh, "The effect of size on photodiode pinch-off voltage for small pixel CMOS image sensors," *Microelectron. J.*, vol. 40, no. 1, pp. 137–140, Jan. 2009.

CHEN CAO was born in Xi'an, China. He received the B.S. degree from the School of Physics, Xi'an Science and Technology University, Xi'an, in 2009, and the M.S. degree from the Institute of Microelectronics Technology, Xi'an, in 2012. He is currently pursuing the Ph.D. degree in microelectronics and solid-state electronics with Image Sensor Design Team, Department of IC Design, Institute of Microelectronics Technology. His current research interests include solid-state image sensor pixel design, optoelectronics device modeling and simulation, with particular pinned photodiode-based devices.

BENLAN SHEN received the B.S. degree from the School of Physics and Electronic Engineering, Taishan University, Tai'an, China, in 2011, and the M.S. degree from the Beijing Institute of Technology, Beijing, China, in 2014. She works as an Optical Design Engineer with LUSTER Light Tech. Corporation, Beijing. Her current research interests include solid-state image sensor performance test and the optical system design.

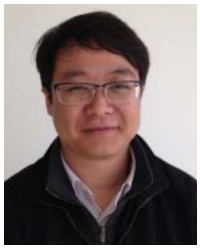

BING ZHANG received the M.S. and Ph.D. degrees in microelectronics and solid-state electronics from Xidian University, Xi'an, China, in 2007 and 2011, respectively. From 2006 to 2007, he was a Research Assistant with the Department of Design, RCL Semiconductors Ltd., Hong Kong, where he researched about the semiconductor device reliability design and test techniques. Since 2012, he has been a Semiconductor Optoelectronics Device Design Engineer with the Image Sensor Design Team, Department of IC Design, Institute of Microelectronics Technology, Xi'an. His current research interests include solid-state image sensor design, pixel design and parameter extracting, and device reliability analyzing.

LONGSHENG WU received the M.S. degree in microelectronics and solid-state electronics and the Ph.D. degree in computer system structure from the Institute of Microelectronics Technology, Xi'an, China, in 1994 and 2001, respectively. He is currently working as a Professor and a Doctoral Supervisor with the Institute of Microelectronics Technology. Since 2005, he has been in charge of a number of the Chinese National Major Projects in the field of digital/analog mixed-signal IC design. Since 2012, he has been the Head of the Image Sensor Design Team, Department of IC Design, Institute of Microelectronics Technology. His current research interests include solid-state image sensors design, hardening device, or circuit design for space applications.

JUNFENG WANG was born in Shaanxi, China. He received the M.S. degree in microelectronics and solid-state electronics and the Ph.D. degree in computer system structure from the Institute of Microelectronics Technology, Xi'an, China, in 1991 and 2012, respectively. Since 2001, he has been a Professor of Analog Circuit Design, Department of Hybrid IC, Institute of Microelectronics Technology, where he is currently a Doctoral Supervisor. His current research interests include digital/analog mixed-signal large-scaled IC design, and modeling and hardening techniques particular for the analog circuit for special environment applications.